Cement and Concrete Research 40 (2010) 4–13

Contents lists available at ScienceDirect

Cement and Concrete Research

journal homepage: http://ees.elsevier.com/CEMCON/default.asp

Microstructural development of early age hydration shells around cement grains

E. Gallucci *, P. Mathur, K. Scrivener

Laboratory of Construction Materials, Ecole Polytechnique Fédérale de Lausanne, CH-1015 Switzerland

ARTICLE INFO

Article history:
Received 5 November 2007
Accepted 18 September 2009

Keywords:
TEM
Early age
Hydration shells
Cement microstructure
C–S–H

ABSTRACT

An important microstructural aspect of the early hydration of Portland cement (PC) is the formation of a shell of hydration products around cement grains. There is, at present, limited information on the mechanism of formation of the shell and of the chemistry of the phases that constitute the shells. Through the use of STEM imaging of early age hydrated cement pastes as early as 2 h, the present work shows that the shells correspond to the first C–S–H type product formed which has a distinct morphology compared to C–S–H formed later when the main reaction occurs (nucleation and growth stage at setting time). The shells form only around the silicate part of the grain and are not empty but filled with a fragile fibrous C–S–H which appears to have a lower (packing) density than the rest of the hydration products. The cement grains underneath the shells are seen to react unevenly and the hydration seems to follow a reaction front, leaving striations up to 1 μm deep on the grains. Over the long term, the original fragile product seems to densify and gives rise to the usual inner C–S–H. High resolution EDS chemical analysis and mappings were used to get insight into the chemistry associated with the formation of these early age products. The C/S ratio of all C–S–H (inner and outer shell) is the same (within the limits of the analysis accuracy) and evolves insignificantly over the first 24 h of hydration. High concentrations of sulfate are associated with the C–S–H formed during the early development of the microstructure, but these decrease later, the sulfate being mainly incorporated into ettringite.

1. Introduction

The hydration of Portland cement is known to be a complex phenomenon. Although the broad pattern of reactions and microstructural development are known, a number of important questions remain unanswered. A major issue concerns the interactions between the different clinker minerals present in Portland cement. The hydration reactions with water are dominated by impure C_3S (alite), which constitutes the majority of Portland cement. However, there are significant differences between the hydration of cement and C_3S and understanding these differences is fundamental to predicting the performance and durability of cementitious systems. From a microstructural point of view, the most obvious difference in the early reactions of cement pastes and pastes of C_3S is the formation of a "shell" of hydration product in the former, separated from the underlying reacting grains.

In the 1970s, Hadley [1] observed the presence of hollow shells of hydration products in fractured cement samples. The youngest specimens studied in which the presence of shells was noted were 1 day old with no appreciable filling of the void between the shell and the grain by 3 days. Their persistence was observed up to at least 28 days. Prior to these investigations, SEM micrographs from various studies of fractured cement samples showed the presence of hydrated shells. However, they were often incorrectly interpreted as places where residual unhydrated cores had been pulled out during fracturing of the specimen [2] or due to drying shrinkage [3].

Scrivener and Pratt [4] studied mixtures of monophased grains of C_3S, C_3A and hemi-hydrate. At 1 day of hydration, they observed a close contact between the C_3S grains and hydration products while there were gaps up to 10 μm between C_3A grains and their hydration shells. This difference in behaviour between cement and mixtures of pure phases shows that the distribution of the anhydrous phases within the cement grains affects the hydration process. On the other hand, Hadley et al. [5] reported that hollow-shell formation is not restricted to cement per se, but occurs to some limited extent with alite alone, and certainly with alite–gypsum and alite–gypsum–C_3A mixtures. This was confirmed by Kjellsen and Justnes [6] who reported the presence of hollow shells in alite pastes at 24 h. In the case of alite, shells are reported to form only around grains smaller than 5 μm, unlike in Portland cement where grains of all sizes have shells around them.

Using wet-cell TEM and SEM-BSE imaging, Scrivener [7,8] observed the formation of an ill crystallised product on the surface of C_3A grains hydrated in the presence gypsum after a few minutes; and nucleation of short AFt rods out in solution. Shell formation in Portland cement was attributed to the growth of outer C–S–H on a network of AFt leaving a gap of a few μm between the grain surface and the shell. Longer rods of ettringite were subsequently observed to form from further hydration of C_3A after the main peak of reaction of the C_3S. Subsequently C_3S continued to react to form inner C–S–H within the shell.

* Corresponding author.
E-mail address: emmanuel.gallucci@epfl.ch (E. Gallucci).

0008-8846/$ – see front matter © 2009 Elsevier Ltd. All rights reserved.
doi:10.1016/j.cemconres.2009.09.015

The objectives of the present study were to provide further understanding about early age shell formation and detailed characterisation of its composition, morphology and structure. Since the phenomenon occurs at the submicron scale, high resolution scanning transmission electron microscopy (STEM) was chosen as the main tool of investigation.

The development of TEM to study hydrated cement paste has been reviewed by Richardson [9]. Early works on crushed and dispersed samples [10–12] failed to preserve the spatial relation of products. This drawback is solved with ion thinning, but the technique is difficult to apply to samples of cement paste which are very fragile and easily damaged during preparation, especially for young samples. This technique was pioneered by Javelas et al. [13] on mature mortars and Dalgeish et al.[14] on mature cement pastes. The first attempt on early age specimens was made by Scrivener [7,15] who used scanning transmission electron microscopy (STEM) to observe the formation of separated shells around reacting cement grains in samples as young as 5 h. Subsequently TEM has been extensively used by Groves [16], Rodger [17] and Richardson [18–20], although these studies have mostly focussed on more mature materials, hydrated for 1 day or more.

Previous research has used almost exclusively bright field imaging, where there is a strong contrast between the solids (unreacted cement grains and hydration products) and pores, but it is more difficult to appreciate contrast differences between the different solid phases. In this work, STEM in dark field mode using a high angle annular detector (scattered beam used to form the image) was chosen so that the contrast between the (bright) solid phases was significantly improved. This contrast mode is also more analogous to that in, now familiar, backscattered electron images in the SEM.

This paper reports the STEM investigation of ion-thinned samples as early as 2 h after mixing with water. Attention was focused on the general microstructural development with a special emphasis on the formation, evolution and morphology of shells together with precise chemical analysis of the various C–S–H observed and their evolution with time up to 48 h.

2. Materials and methods

The cement used in this study was a CEM I 52.5 N from Lafarge. Its phase (XRD-Rietveld) and elemental (XRF) compositions are given in Table 1. Cement paste specimens were prepared at a water to cement ratio of 0.35 (this is equivalent to about 0.45 in concrete). Prior to TEM examination, samples at 2, 4, 6, 8, 10, 12, 18, 24 and 48 h of hydration were dried, impregnated and polished. The free water was removed by freeze-drying (freezing of the paste in a mixture of ethanol and solid CO_2 [−80 °C] followed by sublimation of the frozen water at low pressure and low temperature). Once dried, the specimens were epoxy impregnated. A cylindrical disc about 1 mm thick and 2.5 mm in diameter was then taken out from the centre of the bulk sample and was mechanically polished using the tripod method down to a thickness of about 10 µm. It was then glued on a slotted grid and ion milled (argon ions) at 2–2.2 keV until electron transparency was achieved (interference fringes seen under optical microscope). Finally, samples were coated with a layer of carbon a few nanometers thick to make them electrically conducting to avoid damage due to charge accumulation.

Imaging was done using a HF2000 Field Emission Gun Scanning Transmission Electron Microscope (FEG-STEM) fitted with an EDS analyser at a high take off angle for efficient collection of the X-rays. This enabled analyses to be made without tilting the specimen. The operating voltage was 200 kV and the current at the sample surface was estimated to be about 1 nA. STEM makes it easier to obtain high magnification images without beam damage. Most of the images were acquired in the dark-field mode, with a high angle annular detector fitted in the microscope; this improves contrast for low atomic weight materials such as cement. Chemical mapping was done in a CM300 (FEG-STEM) at an operating voltage of 300 kV while tilting the samples to around 10°.

EDS spectra were acquired using an Oxford spectrometer/Inca system. Due to the high water content of the hydration products, it is difficult to obtain local chemical analyses without severe beam damage and volatilisation of hydration products, especially C–S–H and ettringite. A successful approach was developed to avoid specimen damage: the desired feature of the microstructure was magnified to a few hundred thousand times such that it covered the whole of the observation screen; a small area approximately 20 × 20 nm was then scanned while giving a large defocus to the beam. This completely avoided material loss and gave satisfactory results.

Table 1
Phase (XRD Rietveld) and elemental (expressed as oxide) composition of the cement.

XRD		XRF	
Phase	wt.%	Oxide	wt.%
C_3S	62.5 ± 2.0	CaO	65.49
C_2S	16.4 ± 1.0	SiO_2	20.58
C_3A (cubic)	7.5 ± 1.0	Al_2O_3	4.92
C_3A (orthorhombic)	1.8 ± 0.4	Fe_2O_3	1.83
C_4AF	3.2 ± 0.5	SO_3	3.76
$CaSO_4 \cdot 2H_2O$	2.3 ± 0.4	Na_2O	0.14
$CaSO_4 \cdot 0.5H_2O$	1.8 ± 0.4	K_2O	0.24
$CaSO_4$	1.1 ± 0.4	MgO	1.00
CaO	0.0 ± n.s.	TiO_2	0.22
MgO	0.5 ± n.s.	L.O.I.	1.82
$Ca(OH)_2$	0.0 ± n.s.		
$CaCO_3$	2.0 ± 0.4		
K_2SO_4	0.9 ± n.s.		

n.s. – not significant – phase content below reliability limit.

3. Results and discussion

3.1. Early age microstructural development — shell formation.

After 2 h most of the grain surfaces appear “clean” with no sign of dissolution or deposition of hydrates. Occasionally, a few diffuse hydration products are observed as on the right side of the central grain in Fig. 1. EDS elemental maps show that these primarily contain calcium and sulphur together with small amounts of aluminium. No silicon was detected at all. Although the morphology is rather indistinct, small geometrical features are observed which could be crystals of AFt[1] (or A.Fm) as reported by Minard et al. in the early hydration of C_3A [21]. Because of the high sulphur level observed, some of these regions could correspond to un-dissolved calcium sulfate particles.

The earliest time at which distinct shells were seen is 4 h when they seem to consist of a thin layer (a few tens of nm) of dense C–S–H

[1] From [22]: The term AFt (Al_2O_3–Fe_2O_3–tri) refers to $C_3(A,F).3CX.yH$ type phases in which X is a doubly charged anion (sulfate, carbonate) and $30 \le y \le 32$. The term ‘tri’ relates to the 3 units of CX. AFm (Al_2O_3, Fe_2O_3-mono) refers to $C_3(A,F).CX_2.yH$ type phases where X is a singly charged anion (OH^-) or half a formula unit of a doubly charged anion (SO_3^{2-}, CO_3^{2-}) and y generally <20. The term ‘mono’ relates to the single CX_2 unit. The nature of AFm phases in cement is much more diversified than in AFt with e.g. calcium monosulfo-aluminate, calcium monocarbo-aluminate, Friedel's salt, etc. In this work, in all instances, AFt and AFm will respectively refer to ettringite and mosulfoaluminate (eventually with iron substitution in place of aluminium in Section 3.4).

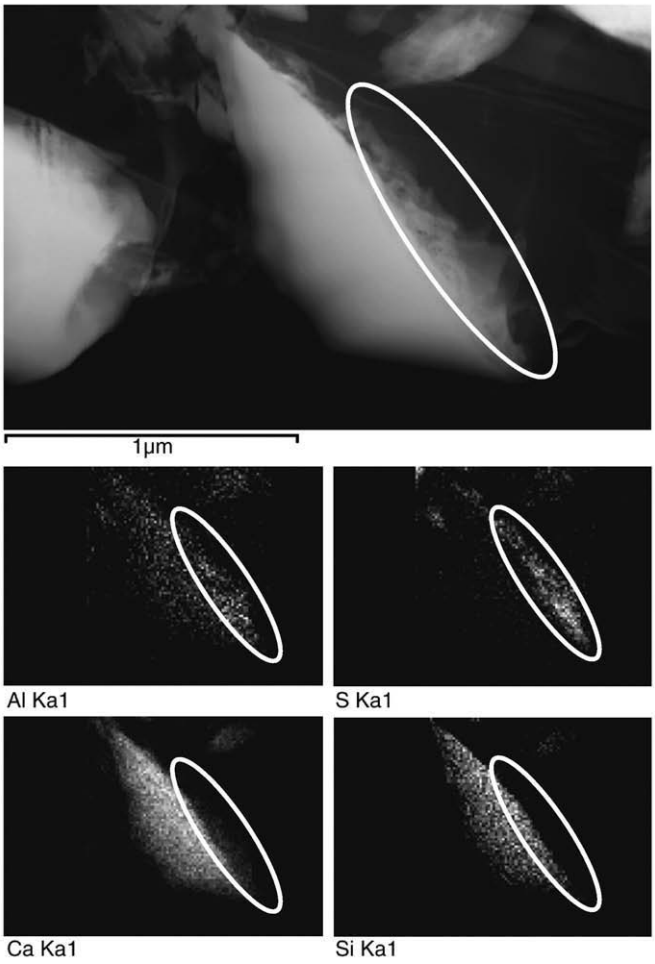

Fig. 1. EDS elemental mapping at 2 h of hydration: only a few diffuse hydration products (in white circle) are observed at the surface of some grains. These mainly consist of aluminium, sulfur and calcium as seen in the EDS mappings (bottom).

product (Fig. 2), oriented parallel to the original surface of the grain. By 6 h, shells are formed either partially or fully around the grains and are connected with other parts of the hydrating matrix through outer C–S–H. After this, they do not change much with time and seem to act as a support for the deposition of both inner and outer C–S–H on either side. A sequence of images showing the evolution of the shells at various ages is shown in Figs. 3 and 4. The gaps between the shells and the dissolving grains are not empty but are filled with a fragile, fibrous C–S–H rich product which connects the shell and the grain surface.

After 24 h of hydration, the shells fill in rapidly with a dense homogeneous product whose morphology is similar to the inner

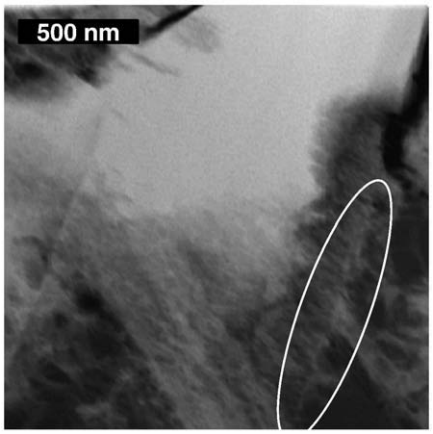

Fig. 2. Formation of the first shells after 4 h of hydration (in white circle). It is oriented parallel to the original surface of the grains, orthogonally to the fibrous product generated by the dissolution of the alite grain.

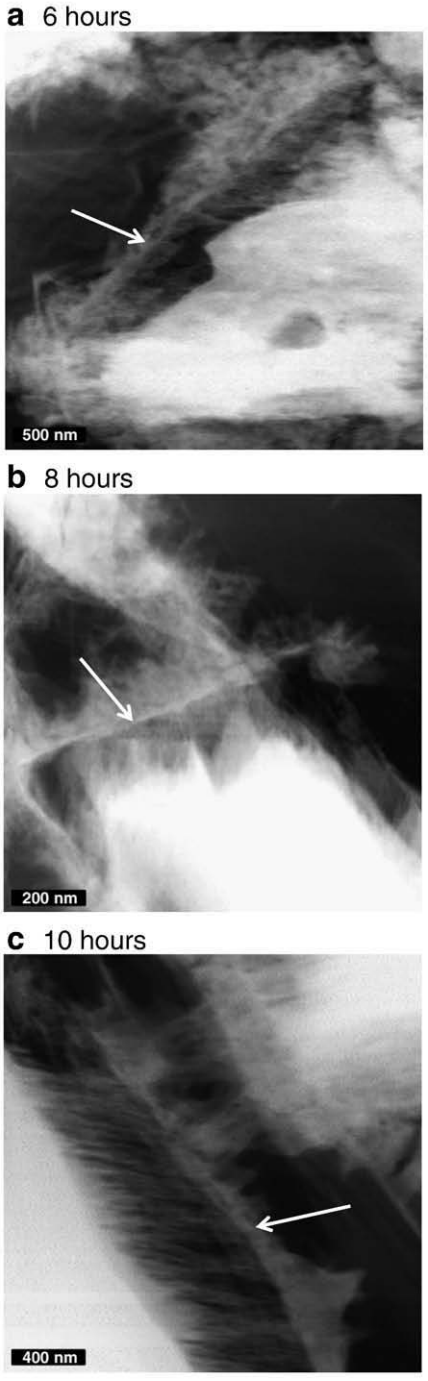

Fig. 3. Evolution of the shell with time : once formed the shell does not change much with time and acts as a support for the deposition of both inner and outer C–S–H on either side (white arrows point to the shell/bright masses are alite grains/in between: fragile inner product).

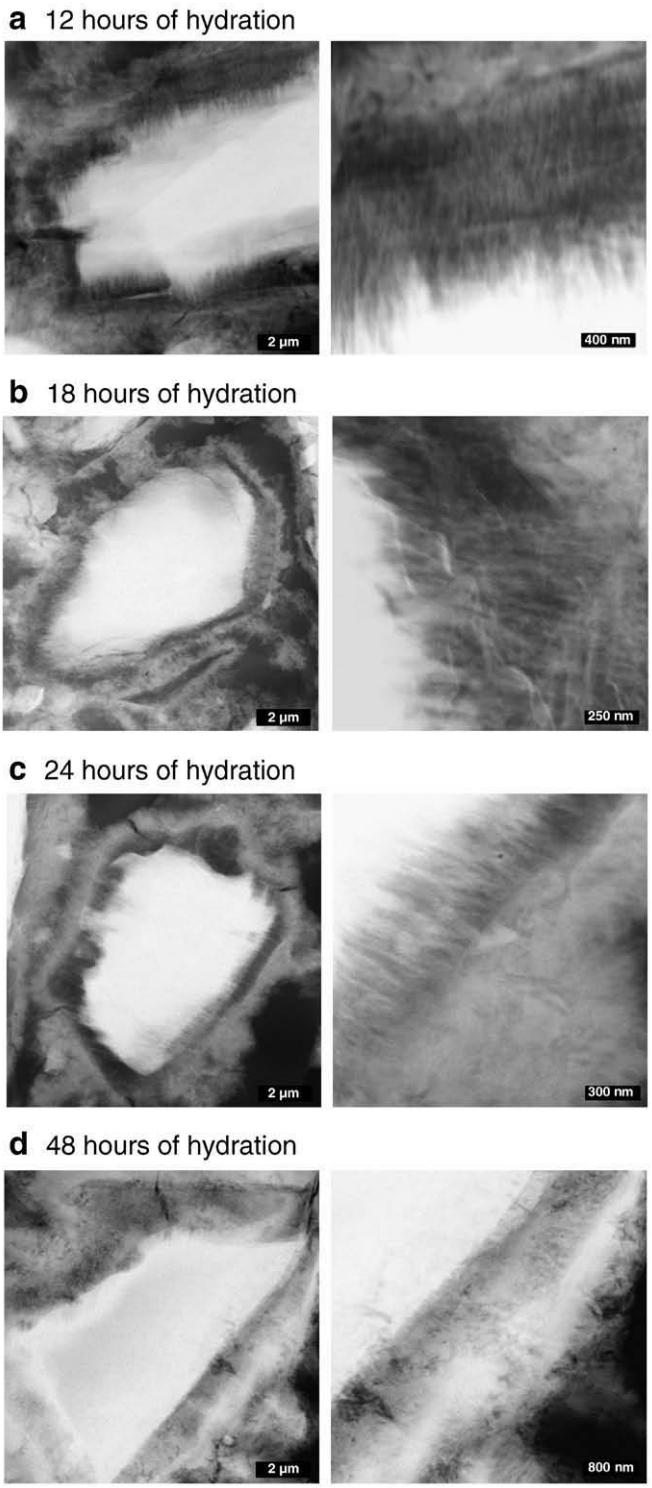

Fig. 4. Microstructural development: in-filling of shells and compaction of the inner product.

product generally observed in SEM-BSE micrographs of polished sections. Rather than a change in the nature of the product, it seems that this dense hydrate results from an infilling or compaction of the fragile early age inner product inside the shell (Fig. 4c and d).

Whatever the age of the specimen the shells form nearby the silicate parts of the grains but not in the vicinity of alumino-ferrite (Fig. 5). Chemical analyses and mappings show principally calcium and silica with a ratio appropriate for C–S–H (Section 3.3) but large

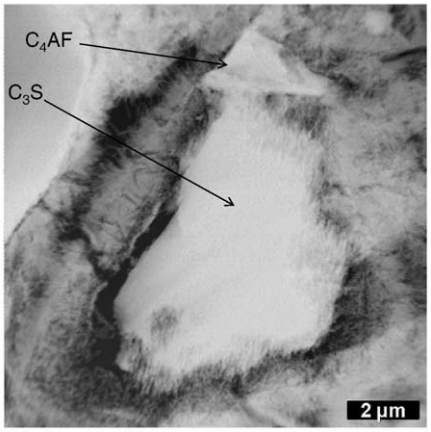

Fig. 5. Preferential formation of the shell around silicates: the undissolved alumino-ferrite (top of the grain) is partly covered by outer C–S–H but no distinct shell is seen. The shell around the silicate part of the grain (bottom) stops disrupts in the vicinity of the alumino-ferrite (specimen at 24 h).

amounts of sulfur (as sulfate) are also systematically detected (Fig. 6 and Section 3.3) while the analyses are almost always aluminium free.

The phenomenon of shell formation was observed for most of the grains and does not seem to depend on the grain size or shape. At a given age, closer examination indicates that in all instances the shell lies at more or less the same distance from the grain surface and can thus be imagined as a 3D surface which has approximately the original shape of the grain it encloses.

The observations also show that once a shell has formed, the surface of the reacting grain underneath is very rugged (e.g. Figs. 4 and 5); dissolution seems to occur preferentially in some areas and gives rise to sharp ridges a few tens of nm in thickness. This profound "etching" of the surface which is certainly related to certain crystallographic orientations starts between 2 and 4 h of hydration and increases progressively up to 600 nm at 12 h and eventually 1 µm at 24 h in some instances. This clearly shows that the reaction of cement grains proceeds by the inward movement of a reaction front and indicates a preferential reaction along certain planes. After around 24 h of hydration, together with the compaction of the inner product within the shell, the deep etching of the grain surface seems to decrease somewhat and this surface comes into close contact with the inner product layer.

Similar effects of selective reactivity can in fact be seen in previous studies [e.g. Ref 8 Figs. 11 and 13]. Menetrier [23] also showed the formation of edge pits on alite surfaces and Fierens [24] found that the hydration rate is sensitive to the density of defects of the crystals. More recently, Juilland et al. [25] demonstrated, by analogy with the dissolution theory of crystals that alite dissolution proceeds mainly by the formation of edge pits and step retreat mechanisms. It is therefore highly influenced by its internal crystallographic and surface defects at the origin of such uneven dissolution fronts.

3.2. Morphology of hydration products

Many authors [e.g. 9,22,26] report the difference in C–S–H morphology between outer product, which forms in the space originally occupied by water and has an open fibrillar or foil-like morphology; and inner product, which forms in the space originally occupied by the anhydrous grains and has a dense, homogeneous morphology.

The morphology of the outer product observed in this study at early ages is as reported previously. However, at early ages the inner product is fragile (Figs. 2 and 3) with a low packing density. It later densifies to give the usual inner product morphology. The morphology of the fragile product appears to be related to the selective

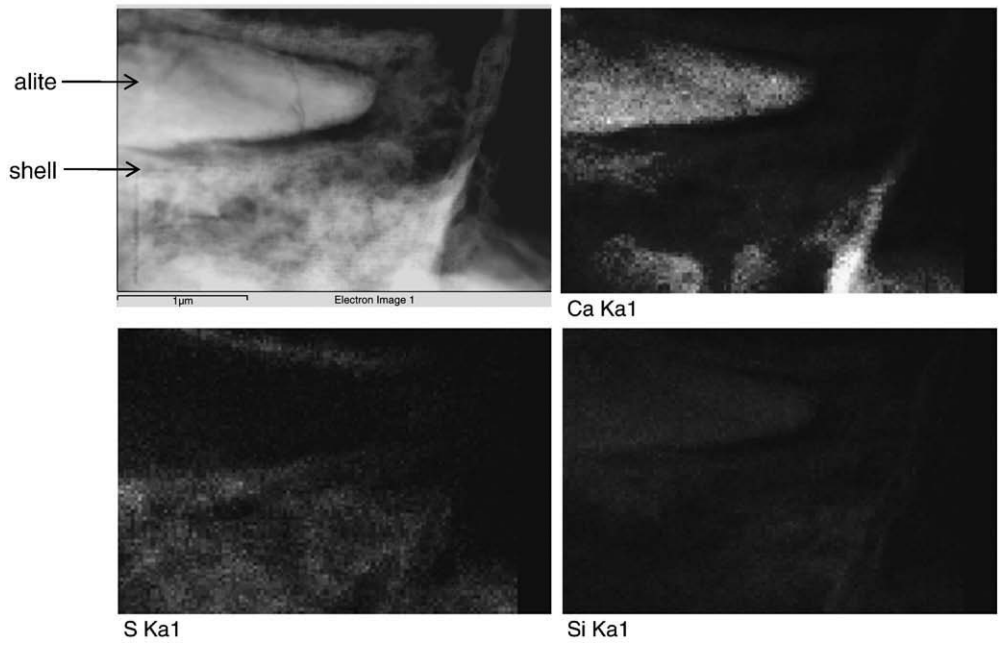

Fig. 6. EDS Elemental mapping at 6 h of hydration showing the association of calcium, silicium and high levels of sulfur in the shell.

reactivity of alite: it seems to be connected to the dissolving ridges. The morphology could be interpreted as fibres or perhaps "strings" of nanocrystals, which continue the orientation of the etch strata (Fig. 7). After densification (or compaction) at around 48 h the morphology of the inner product appears similar to that of the shell. Other instances of low density inner product have already been reported in previous studies but they certainly do not correspond to that observed here: they generally concern small grains totally consumed (a kind of Hadley grain) in which the internal void is gradually filled with product that should thus rather be considered as being outer C–S–H in terms of morphology and growth mechanism but certainly not as inner product as usually admitted and for which growth is fed by the dissolving embedded grain.

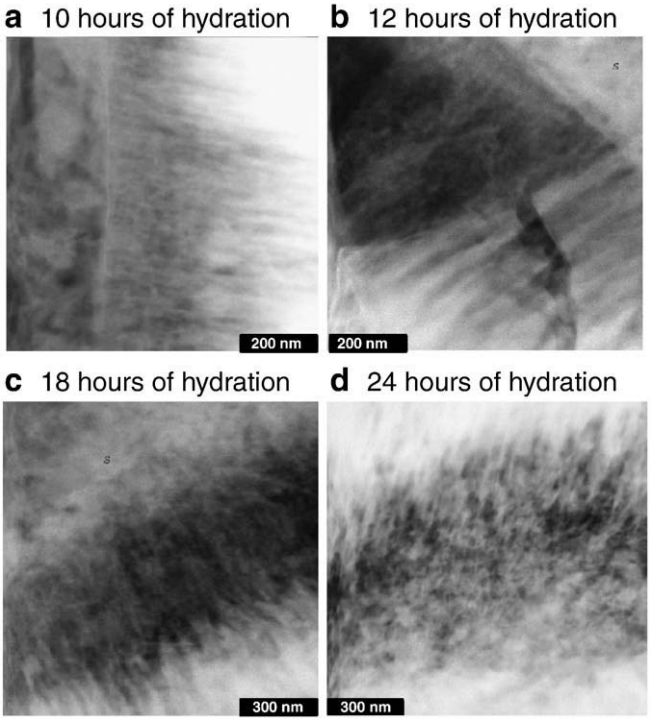

Fig. 7. Fibrous/particulate nature of the early age fragile inner product.

On the other hand the "shell" has its own particular morphology: contrary to the outer and inner products whose "densities" (or packing fraction) seem to be lower when the space available for their growth is larger, the shell shows, right from its formation, a clear dense packing. It extends around most of the surfaces of most of the grains and has already formed by 4 h of hydration (i.e. much before any other visible and identifiable C–S–H) for the cement pastes studied here. It mainly consists of a thin dense layer apparently oriented along the original surface of the grain, which thickens slightly with time up to about 50 nm (Figs. 2 and 3) and seems to be the substrate on which the outer product grows e.g. Figs. 3–5 (whether it acts as nucleation site or simply as substrate for deposition is not resolved here).

Despite its dense appearance, the shell must clearly remain highly permeable since the continuous formation of more products both inside and outside the shell indicates significant transport of water and ions through it. Although not the purpose of the present article, this seems to contradict the conventional explanation for the decrease in rate of cement hydration after the first few hours as being due to diffusion through a hydrate coating [27].

The data collected here bring new insight on the shell formation and allow us to make some hypotheses about its mechanism, although this question cannot be fully addressed here. The mechanism of formation of the shells is certainly different from that of both the inner and outer products, as its morphology, density and orientation are "singular". There are in fact very few studies which have experimentally reported any characterisation of C–S–H at such early ages. Zingg et al. [28] recently observed by cryo-FIB cross section imaging a discontinuous hydration layer after only 25 min of hydration, while Rodger et al. [29] showed that right from the first hours of hydration only monomeric silicate anions are detected in the solid hydrates and these persist over the long term as a 40 nm thick layer around the grains, which could correspond with the shells observed. However it really seems like the shell that we observe correlates closely with the

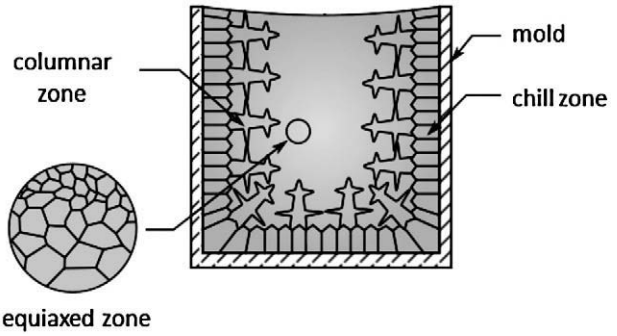

Fig. 8. Tentative analogy between the shell and the chill zone formed during metal casting: the chill zone corresponds to small crystals densely packed at the surface of the mold, on which larger crystal grow (columnar zone). In the case of cement, the columnar zone corresponds to outer C–S–H which grows outwards since the bulk of the shell is already filled with the poorly dense fragile inner product. (figure adapted from http://en.wikipedia.org/wiki/Casting_(metalworking) under GLPL license).

original surface of the grain and is probably constituted of small C–S–H nuclei, some of which then grow out into the solution. In this sense it is analogous to the formation of the chill and columnar zones in metallic castings, shown in Fig. 8. The question of why material moves to the outside of the shell remains unanswered, but this is less of a mystery when it is realised that the gap between the shell and the grain does in fact contain solid products with a low packing fraction.

3.3. Chemical composition of C–S–H

Despite the high spatial resolution (of the order of 10–20 nm^2) of our imaging system, Al, Fe and sulfur were often found in the "C–S–H" analyses. This shows either the fine intermixing of C–S–H with sulfur, Al and/or Fe rich hydration products or absorption of these ions at the 'nano' scale. EDS analysis spots were chosen carefully depending on the morphology of the hydrated phases probed, so that results could be attributed the most accurately possible to pure phases. The data obtained have been processed and sorted as being representative of almost pure outer C–S–H, pure inner C–S–H, pure shell and phase intermixing in the matrix (outside the shells where the intermixing of outer C–S–H with other phases was obvious).

Regarding the three categories of C–S–H identified and for all ages investigated here, results showed, quasi-systematically, C/S ratios ranging from around 2 to 3.5 (very high!) with, in addition, very high levels of sulfates but with no detectable aluminium in almost all instances (e.g. Fig. 9). The absence of aluminium tends to show that the C–S–H formed in the vicinity of the grains at these early ages:

1) contains more than just lime and silica, but has little or no intermixed AFt/AFm phases and
2) shows almost no substitution of Si^{4+} by Al^{3+} as seen at later ages when the mean length or 'degree of polymerisation' of the silicate anion chains in C–S–H increases.

Although such measurements were not done in the framework of this study, this fits quite well with the results of Rodger et al. [29] who observed only mono- and dimeric hydrated silicates in the first few hours of hydration with therefore very little probability of Al^{3+} bridging site occupancy.

The high C/S ratios measured were interpreted as being due to one or more of the following:

- the fine intermixing of portlandite nano-crystallites in the C–S–H (supported by the trend of analyzed spots towards CH in Fig. 7-left),
- residual un-dissolved calcium sulfate particles (trend towards $C\hat{S}H_x$)
- the coexistence of tobermorite (T2) and jennite (J2) like structures.

The latter proposition derives from measured bimodal C/S distributions in early age pastes [18] which were later interpreted as equal mixtures of tobermorite – (C/S = 1.25) and jennite – (2.25) based units [19]. However, the actual measured values (around 1.7 and 2.0) in these bimodal distributions differed significantly from the theoretical values and in the present case this would imply a strong displacement towards almost pure jennite-like C–S–H. Regarding the two first propositions, electron diffraction checks done on some of these specimens did not show significant diffraction patterns of peaks for either CH or $C\hat{S}H_x$. Sulfur (presumably as sulfate) was therefore hypothesised to be adsorbed on C–S–H and it is thought that this adsorption entails the coupled uptake of Ca^{2+} (being primarily adsorbed on highly negatively charge C–S–H surface) and SO_4^{2-} (as a counter ion) ions to preserve electrical neutrality. Such high levels of adsorbed sulfate have recently been shown and explained by experiments and Monte Carlo simulations [30] but this was already suggested by Odler [31] based on the results of TGA and wet chemistry titration experiments on C_3S pastes in which the content of sulfate in the C–S–H increased with the amount of calcium sulfate initially added. Based on his results, Odler stated that those sulfate ions were unlikely to be firmly bound to the C–S–H structure but rather physically adsorbed and later on released. In the present case, this coupled adsorption would account for the high SO_4^{2+} levels measured on one hand and part of the excess Ca^{2+} ions measured with respect

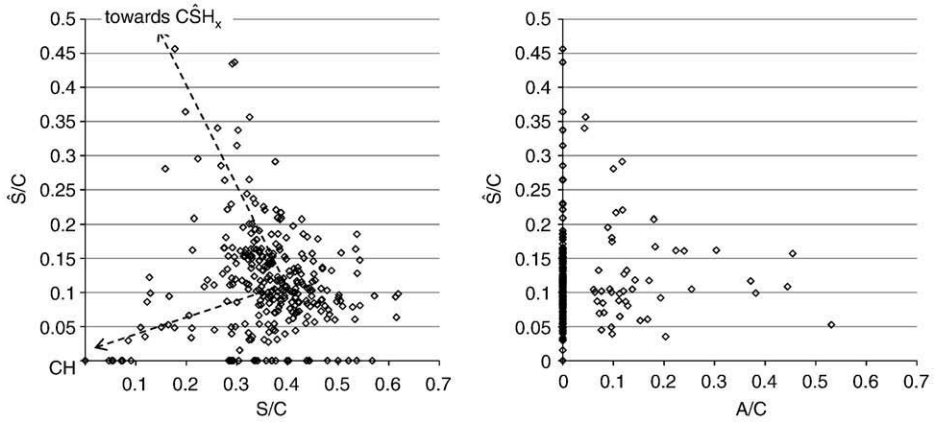

Fig. 9. Composition of C–S–H (indistinctly inner-, and outer-shell) after 10 h of hydration (233 analysis). The very few points containing Al^{3+} ions (right plot) correspond mainly to intermixed AFt. More than 90% of the points are Al^{3+} free but show very high levels of sulfates. The trends of phase intermixing are probably C–S–H/CH and C–S–H/CŜ.

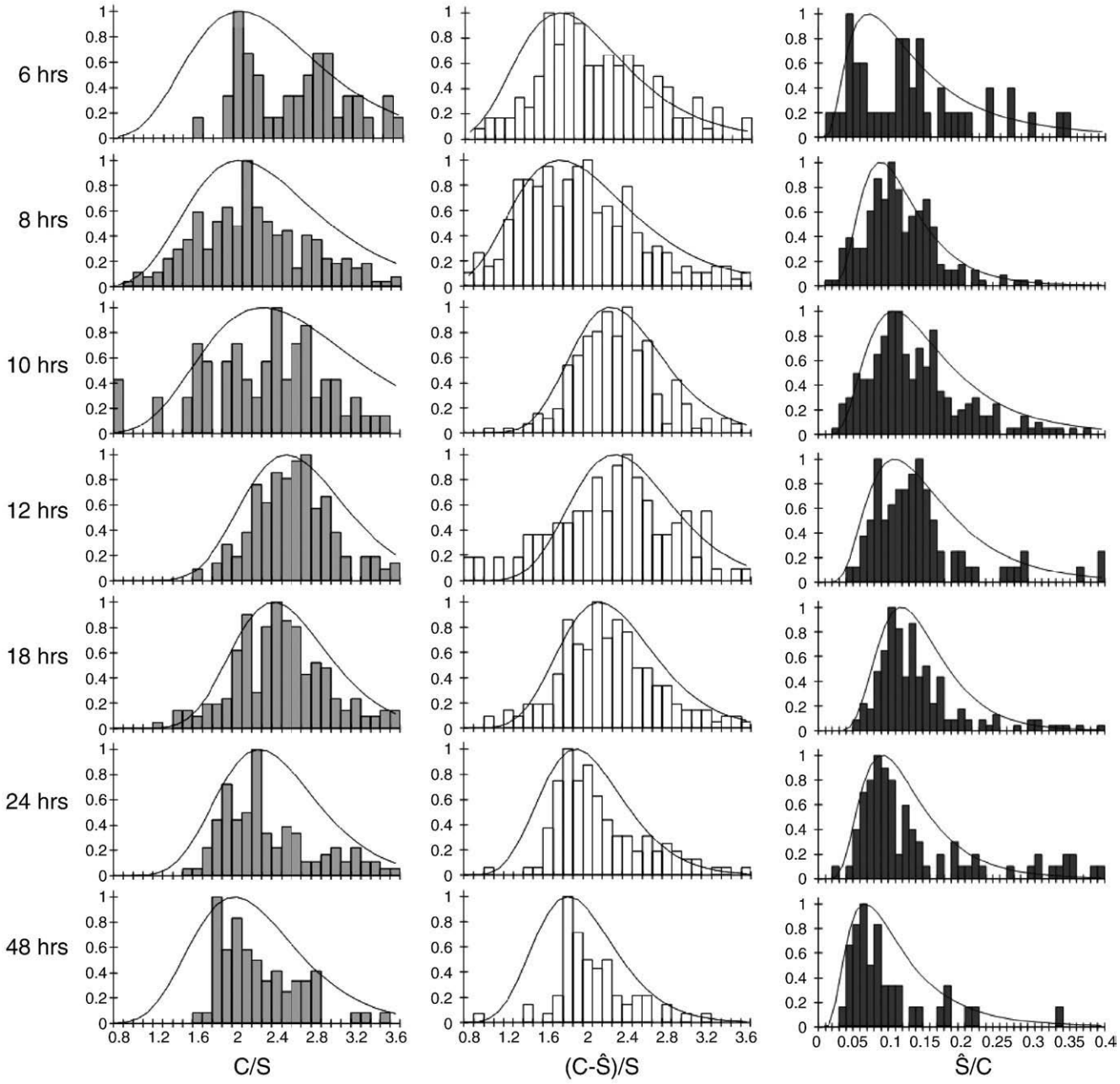

Fig. 10. Evolution of the distributions of C/S, (C–Ŝ)/S and Ŝ/C ratios in C–S–H (indistinctly inner-, and outer-shell) with time. Black trends are log-normal laws calculated from the measured distributions (modes, confidence intervals and number of analyses given in Table 2).

to C–S–H. Fig. 10 gives the evolution of the distributions of C/S and (C–Ŝ)/S ratios (which assume this coupled 1:1 adsorption) between 6 and 48 h. The black trends fitting the distributions are the log–normal laws calculated from the collected data. Statistically those distributions were more satisfactorily fitted (lower standard deviation and lower half width) for (C–Ŝ)/S than C/S which confirms the contribution of both Ŝ and C extra atoms to the C/S ratio. Furthermore, the (C–Ŝ)/S ratios clearly show much closer values to the typical ratios of C/S for C–S–H (Fig. 11 and Table 2).[2] The evolution of the C/S ratio shows a strong increase until between 12 and 18 h of hydration (probably more or less up to the time of maximum heat release of the reaction) and then decreases back to more regular values of around 2. The evolution of the (C–Ŝ)/S follows more or less the same trend but with a lower relative increase which corresponds to the increase in sulphur level measured (Fig. 11). The fact that the (C–Ŝ)/S ratio changes with time shows that the high C/S measured cannot be explained only by a 1:1 co-adsorption of C and Ŝ (assumed here). Besides other effects such as those suggested above (e.g. intermixed nanocrystalline CH), it is also possible that there is absorption of more calcium than only that coupled with sulfate (presumably equivalent to the adsorption of $CaOH^+$ groups).

Although calcium sulfates are primarily added to cement to control the rapid hydration of C_3A, they also influence the hydration of alite [e.g. 22,32–34], such that there is an optimum sulfate addition which

[2] In Fig. 10 and Table 2, modes of the log-normal distributions rather than their average are given since the mode [$\exp(\mu-\sigma^2)$] considers the scattering of the data (through σ) and gives a better average statistical figure of the distribution. Confidence intervals rather than standard deviation (σ) are given to take into account the dissymmetry of the distribution.

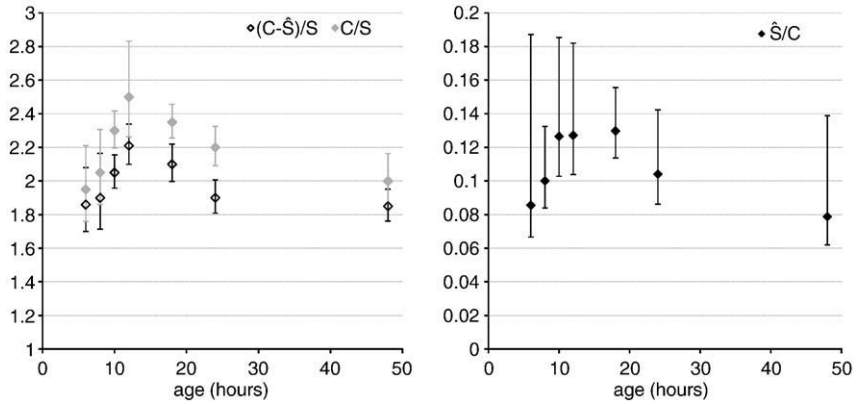

Fig. 11. Evolution of the C/S, (C–Ŝ)/S and Ŝ/C ratios in C–S–H (indistinctly inner-, and outer-shell) with time. (modes of the distributions in Fig. 8 and confidence intervals at $\pm\sigma$ as given in Table 2).

gives the highest strength. Generally, calcium sulfate dissolves rapidly upon addition of water and its concentration in the solution remains constant over the first few hours, while a reserve of solid gypsum remains. When the solid sulfate source is exhausted, after about 1–2 days, the concentration in solution drops dramatically, followed by a renewed growth of ettringite and later on the precipitation of calcium aluminate mono sulfate (or eventually mono carbonate) [4,22].

In the present study, sulfate was found to be well distributed in the hydrating matrix, essentially adsorbed on C–S–H as discussed above but also occasionally present in the form of short ettringite rods. Fig. 10 shows the evolution of the distributions of Ŝ/C ratios while Fig. 11 and Table 2 give the modes and standard deviations of the log–normal laws they fit. Despite the large error bars, these show that up to 12 h (and probably even later) the coupled uptake of SO_4^{2-} and Ca^{2+} increases continuously to reach a level of 1:7 of extra Ca^{2+} ion which is in the range of values already measured by Odler [31]. From 18 h, the content of Ŝ measured decreases drastically and this corresponds to the time by which several coarse ettringite needles are seen growing from the shell inwards (Fig. 12). This seems to indicate a renewal of the reaction of the aluminate phase and it appears, in accordance with the view of Odler [31] that after the depletion of solid gypsum the renewed reaction of C_3A can continue to form ettringite drawing on the sulfate adsorbed in the C–S–H.

3.4. Intermixing of phases outside the shells

Fig. 13 gives the evolution of the phase intermixing in the matrix outside the shell. These measurements correspond to spots in which intermixed phases could have been present. The data have been sorted and grouped according to the time period i.e. very young specimens on one hand and specimens older than 12 h in the other. In both cases many points remained aluminium free which shows once again the strong CŜ–C–S–H intermixing or sulfate adsorption on C–S–H.

The first group (young specimens) clearly shows a phase assemblage between C–S–H, AFt, and eventually CŜ at 6 h. After that, a clear trend towards C_4AH_x[3] is observed while it seems that high Ŝ content phases (e.g. CŜ) are no longer detected. Although rarely identified, the presence of C_4AH_x in early age hydrate phase assemblages has already been shown in C_3A pastes by Raman spectroscopy [35] but also on model cements by XRD and SEM-EDS[36]. To our knowledge, its presence in real OPC has never been reported and is certainly related to the original Ŝ/A ratio in the un-hydrated cement. The time by which this phase is observed correlates quite well with the maximum adsorbed sulfate in the C–S–H and this tends to confirm that most of the sulfate either dissolves and stays in solution or is involved in other phases (e.g. adsorbed on C–S–H) but is not fully available to react with C_3A which then forms non-sulfated AFm phases. After 12 h, when the content of Ŝ in C–S–H starts to decrease, the phase assemblage in the matrix changes and shows the more usual C–S–H/AFt/AFm (calcium monosulfoaluminate) phase intermixing.

3.5. Presence of iron within hydration products

Although not the prime purpose of this work, in some instances iron was detected in hydration products while at early ages ferrite phases in OPC are generally believed to be less reactive than other anhydrous phases. Although substitution of iron in the AFt and AFm phases can be quite large in materials synthesised in the laboratory, the extent to which it occurs in the highly alkaline environment of cement paste is not well known, but usually considered to be low. Therefore the data obtained in this study are reported as well here. The number of analyses is limited as it was rather difficult to find these pure phases (especially AFt and AFm) at such early ages.

EDS chemical analysis show that small amounts of iron are present in the "C–S–H" as early as 6 h of hydration (Table 3). Iron is only found to be present on or within the shell up to 12 h, with a clear absence outside the shell, except for the very few cases where it is seen close to C_4AF grains. Otherwise, the levels of iron seem to remain low and constant at all ages.

The substitution of iron measured in AFt and AFm phases is shown in Table 4. Up to 12 h no iron is found in these phases but at and after 18 h, almost 30–40% of Al^{3+} is replaced by Fe^{3+} in AFt where it has been clearly detected (a bit less for AFm). The iron substitution level seems to be more or less the same for the two phases and the trends occur at about the same time (18 h). This could indicate an increased reaction of the ferrite phases at around 18 h. But there again, the number of analysis remains quite low and are not statistically representative of any conclusion other than that iron can replace aluminium in Aft and AFm

Table 2
Early age evolution of the composition of C–S–H.

Age (h)	C/S	(C–Ŝ)/S	Ŝ/C	*n*
6	1.95 (0.19–0.26)	1.86 (0.16–0.22)	0.086	63
8	2.06 (0.18–0.26)	1.90 (0.18–0.26)	0.100	272
10	2.31 (0.10–0.12)	2.06 (0.09–0.11)	0.126	233
12	2.50 (0.24–0.33)	2.21 (0.11–0.13)	0.127	133
18	2.36 (0.09–0.11)	2.09 (0.10–0.12)	0.130	212
24	2.22 (0.11–0.13)	1.92 (0.09–0.11)	0.104	120
48	2.01 (0.13–0.16)	1.84 (0.08–0.10)	0.079	81

Modes of the log–normal distributions.
In brackets: disymetric confidence intervals at $\pm\sigma$.
n: number of analysis.

[3] C_4AH_{19} or C_4AH_{13} depending on the saturation state of the specimen [36].

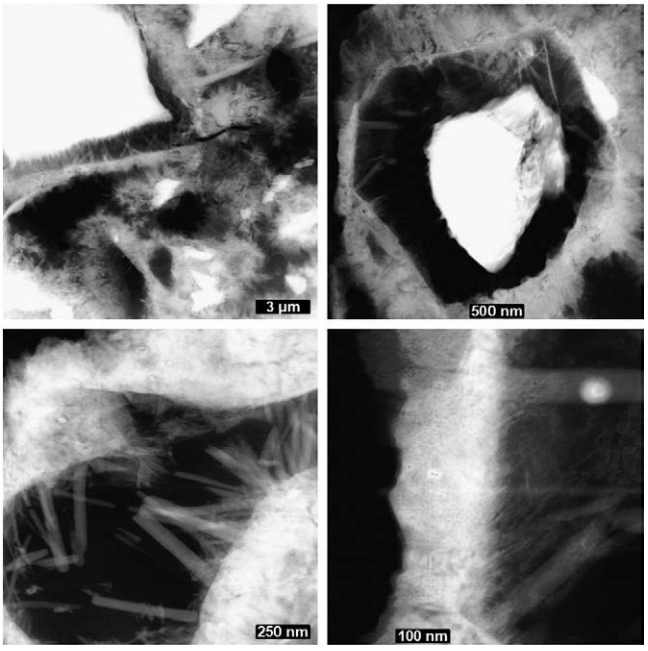

Fig. 12. Examples of the second burst of ettringite formation associated with the depletion of sulfate in the C–S–H. Large rods of ettringite are seen growing inwards the shells (specimen at 24 h).

Table 3
Iron levels (F/C) observed in C–S–H type products (AFt and AFm excluded).

Age (h)	Ip		Shell		Op	
6	0.02 ± 0.01	(3)	0.02	(1)	–	(0)
10	0.03 ± 0.01	(8)	0.02 ± 0.01	(7)	–	(0)
12	0.03 ± 0.01	(4)	0.03	(1)	0.08 ± –	(1)
18	0.05 ± 0.02	(14)	0.04	(4)	0.03 ± 0.02	(6)
24	0.05 ± 0.02	(8)	0.04 ± 0.01	(6)	0.02 ± 0.01	(7)
48	0.04 ± 0.01	(5)	–	(0)	–	(0)

Means and standard deviations.
Number of analysis having iron in brackets.

Table 4
Solid state substitution of aluminium by iron in ettringite and monosulfate.

	AFt		AFm	
Age (h)	P_F/T_{AFt}	(Fe/Al) average	P_F/T_{AFm}	(Fe/Al) average
8	0/10	–	0/0	–
10	0/05	–	0/0	–
12	0/06	–	0/0	–
18	1/04	0.43 ± 0.00	2/2	0.37 ± 0.0
24	8/20	0.33 ± 0.11	0/1	–
48	5/10	0.28 ± 0.08	4/5	0.23 ± 0.04

P_F: analysis containing iron.
T_{AFt}: number of analysis corresponding to pure Aft.
T_{AFm}: number of analysis corresponding to pure AFm.

phases at early age and that the substitution level is necessarily higher than 1:4.

4. Conclusions

TEM specimens as early as 2 h old were successfully prepared and imaged using STEM in dark field imaging mode. This has provided new insights on the early microstructural development at the nanoscale, particularly on the formation of shells.

It was shown that the shells form around the silicate part of the grains between 2 and 4 h of hydration i.e. during or at the end of the induction period. They have a thickness of a few tens of nm and are rather dense compared to usual fibrous C–S–H. They form at the surface of the alite grains and are progressively covered with fibrous outer C–S–H on their outward face and remain linked to the reacting grain through a low density fragile inner C–S–H product i.e. they are not empty as previously believed. Although the exact chemical mechanisms behind the shell formation are still not clear, comparison with phenomena well known in the solidification of metal castings lead us to think that it is composed of small particles of C–S–H which nucleate on the surface of the alite grains and only some of these grains are able to grow out into the solution, forming the low density outer product.

Underneath the shell, alite grains do not react evenly and show a strong etching of their surface up to 1 µm deep which indicates a preferential reactivity. There seems to be some kind of continuity between the alite reacting planes and the fragile hydrated product that forms inside the shell. The mechanism by which this product forms and its correlation with the dissolving ridges of the alite particles should be investigated in greater depth.

Regarding the chemistry of hydration products, the C/S ratio (once the assumed coupled absorption of Ca^{2+} and SO_4^{2-} is taken into account) is the same in the inner product, the shell and the outer product. It increases significantly from 6 to 12 h and then decreases drastically to usual early age C–S–H compositions around C/S 1.9. The high calcium contents observed have been primarily attributed to a co-adsorption of Ca^{2+} and SO_4^{2-} ions. However, even when this contribution is subtracted, the C/S still changes slightly with time, so there may be some other synergetic contributions such as the presence of nanocrystals of CH (not detected by electron diffraction) or the presence of short silicate chains jennite type C–S–H. It is also

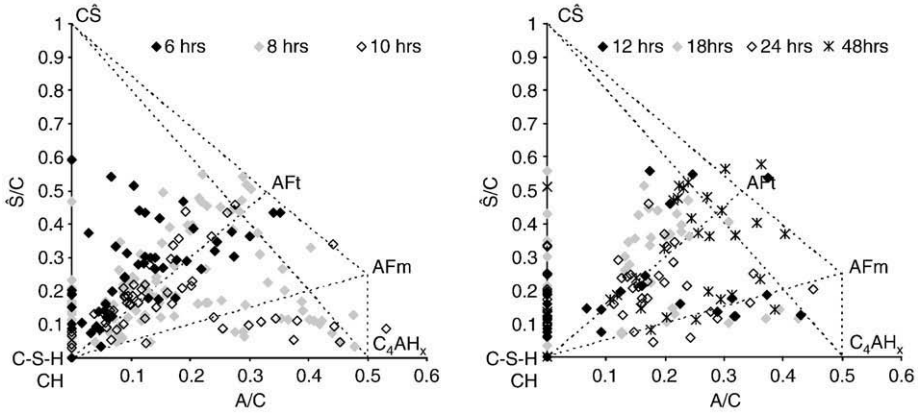

Fig. 13. Evolution of phase assemblage outside hydration shells.

possible that the co-adsorption of calcium and sulfate ions could differ from a ratio of 1:1 which was assumed here. Nevertheless it was clearly shown that high levels of sulfates are adsorbed at early age in the C–S–H and are therefore not available for reacting with aluminates, which in turns allows the precipitation of non sulfated AFm phases (type C_4AH_x). The sudden release of the adsorbed sulfate between 12 and 18 h contributes to the second burst of ettringite formation.

References

[1] D.W. Hadley, The nature of the paste-aggregate interface, PhD thesis, Purdue University 1972.
[2] R.B. Williamson, Solidification of Portland cement, Progress in Materials Science 15 (3) (1972) 279–286.
[3] F.V. Lawrence Jr., J.F. Young, Studies on the hydration of tricalcium silicate pastes I. Scanning electron microscopic examination of microstructural features, Cement and Concrete Research 3 (2) (1973) 149–161.
[4] K.L. Scrivener, P.L. Pratt, Microstructural studies of the hydration of C3A and C4AF independently and in cement paste, Proceedings of the British Ceramic Society 35 (1984) 207–219.
[5] D.W. Hadley, W.L. Dolch, S. Diamond, On the occurrence of hollow-shell hydration grains in hydrated cement paste, Cement and Concrete Research 30 (1) (2000) 1–6.
[6] K.O. Kjellsen, H. Justnes, Revisiting the microstructure of hydrated tricalcium silicate — a comparison to Portland cement and concrete, Composites 26 (8) (2004) 947–956.
[7] K.L. Scrivener, The development of microstructure during the hydration of Portland cement, PhD thesis, University of London, 1984.
[8] K.L. Scrivener, Microstructure of concrete, in: J. Skalny (Ed.), Materials Science of Concrete I, the American Ceramic Society, Westerville, Ohio, 1989, pp. 127–162.
[9] I.G. Richardson, Electron microscopy of cements, in: P. Barnes, J. Bensted (Eds.), Structure and Performance of Cements, 2nd edition, Spon Press, 2002, pp. 500–556.
[10] J.A. Gard, K. Mohan, H.F.W. Taylor, G. Cliff, Analytical electron microscopy of cement pastes: I, tricalcium silicate pastes, Journal of the American Ceramic Society 63 (5–6) (1980) 336–337.
[11] E.E. Lachowski, K. Mohan, H.F.W. Taylor, C.D. Lawrence, A.E. Moore, Analytical electron microscopy of cement pastes: III, pastes hydrated for long times, Journal of the American Ceramic Society 64 (6) (1981) 319–321.
[12] E. Lachowski, K. Mohan, H.F.W. Taylor, A.E. Moore, Analytical electron microscopy of cement pastes: II, pastes of Portland cements and clinkers, Journal of the American Ceramic Society 63 (7–8) (1980) 447–452.
[13] R. Javelas, J.C. Maso, J.P. Ollivier, Réalisation de couches minces de mortier pour observation directe au microscope electronique par transmission, Cement and Concrete Research 4 (1974) 167–176.
[14] B.J. Dalgleish, K. Ibe, Thin-foil studies of hydrated Portland cement, Cement and Concrete Research 11 (5–6) (1981) 729–739.
[15] K.L. Scrivener, P.L. Pratt, Characterisation of Portland cement hydration by electron optical techniques in Electron Microscopy of Materials, Proceedings Material Research Society Symposium 31 (1983) 351–356.
[16] G.W. Groves, P.J. Sueur, W. Sinclair, Transmission electron microscopy and microanalytical studies of ion-beam-thinned sections of tricalcium silicate paste, Journal of the American Ceramic Society 69 (4) (1986) 353–356.
[17] S.A. Rodger, G.W. Groves, Electron microscopy study of ordinary Portland cement and ordinary Portland cement–pulverized fuel ash blended pastes, Journal of the American Ceramic Society 72 (6) (1989) 1037–1039.
[18] I.G. Richardson, G.W. Groves, Microstructure and microanalysis of hardened ordinary Portland cement pastes, Journal of Materials Science 28 (1) (1993) 265–277.
[19] I.G. Richardson, The nature of the hydration products in hardened cement pastes, Cement and Concrete Composites 22 (2) (2000) 97–113.
[20] I.G. Richardson, Tobermorite/jennite- and tobermorite/calcium hydroxide-based models for the structure of C–S–H: applicability to hardened pastes of tricalcium silicate, β-dicalcium silicate, Portland cement, and blends of Portland cement with blast-furnace slag, metakaolin, or silica fume, Cement and Concrete Research 34 (9) (2004) 1733–1777.
[21] H. Minard, S. Garrault, L. Regnaud, A. Nonat, Mechanisms and parameters controlling the tricalcium aluminate reactivity in the presence of gypsum, Cement and Concrete Research 37 (10) (2007) 1418–1426.
[22] H.F.W. Taylor, Cement Chemistry, 2nd edition, Thomas Telford (Eds), London 1997.
[23] D. Ménétrier, I. Jawed, T.S. Sun, J. Skalny, ESCA and SEM studies on early C_3S hydration, Cement and Concrete Research 9 (4) (1979) 473–482.
[24] P. Fierens, J. Tirlocq, J.P. Verhaegen, Luminescence et hydration du silicate tricalcique, Cement and Concrete Research 3 (5) (1973) 549–560.
[25] P. Juilland, E. Gallucci, K. Scrivener, Mechanisms of hydration of cementitious materials at early age, proceedings of the 17th International Conference on Building Materials, Weimar, 2009, session 1.20.
[26] K.L. Scrivener, Backscattered electron imaging of cementitious microstructures: understanding and quantification, Cement and Concrete Composites 26 (8) (2004) 935–945.
[27] S. Bishnoi, Vector modeling of hydrating cement microstructure and kinetics, PhD EPFL n°4093, http://biblion.epfl.ch/EPFL/theses/2008/4093/EPFL_TH4093.pdf (2008).
[28] A. Zingg, F. Winnefeld, L. Holzer, J. Pakusch, S. Becker, L. Gauckler, Adsorption of polyelectrolytes and its influence on the rheology, zeta potential and microstructure of various cement and hydrate phases, Journal of Colloid and Interface Science 323 (2) (2008) 301–312.
[29] S.A. Rodger, G.W. Groves, N.J. Clayden, C.M. Dobson, Hydration of tricalcium silicate followed by ^{29}Si NMR with cross polarization, Journal of the American Ceramic Society 71 (2) (1988) 91–96.
[30] C. Labbez, M. Medala, I. Pochard, A. Nonat, Adsorption of sulfate ions on negatively charged surfaces, In proceedings of the 7th Liquid Matter Conference, Lund, 27 June - 1 July 2008.
[31] I. Odler, Interaction between gypsum and the C–S–H phase formed in C_3S hydration, proceedings of the 7th International Congress on Chemistry of Cement, Paris, vol. IV, 1980, pp. 493–495.
[32] A. Bentur, Effect of gypsum on the hydration and strength of C_3S pastes, Journal of the American Ceramic Society 59 (5–6) (1976) 210–213.
[33] L.E. Copeland, D.L. Kantro, Hydration of Portland cement, Proceedings of 5th International Congress of Chemistry of Cement Tokyo, vol. II, 1969, pp. 387–421.
[34] F.W. Locher, Hydration of pure Portland cements, proceedings of the 7th International Congress on Chemistry of Cement, Paris, vol. IV, 1980, pp. 49–54.
[35] S. Black, G. Breen, J. Yarwood, C.-S. Deng, J. Philips, G. Maitland, Hydration of tricalcium aluminate (C_3A) in presence and absence of gypsum — studied by Raman spectroscopy and X-ray diffraction, Journal of Materials Chemistry 16 (2006) 1263–1272.
[36] A. Quennoz, E. Gallucci, K. Scrivener, Influence of the clinker phase assemblage on the hydration of model cements, proceedings of the 17th International Conference on Building Materials, Weimar, 2009, session 1.21.